Colloids and Surfaces B: Biointerfaces 90 (2012) 159–168

Contents lists available at SciVerse ScienceDirect

Colloids and Surfaces B: Biointerfaces

journal homepage: www.elsevier.com/locate/colsurfb

Spectroscopic and microscopic characterization of biosensor surfaces with protein/amino-organosilane/silicon structure

K. Awsiuk[a], A. Bernasik[b], M. Kitsara[c], A. Budkowski[a,*], P. Petrou[c], S. Kakabakos[c], S. Prauzner-Bechcicki[a,1], J. Rysz[a], I. Raptis[d]

[a] M. Smoluchowski Institute of Physics, Jagiellonian University, Reymonta 4, 30-059 Kraków, Poland
[b] AGH University of Science and Technology, Faculty of Physics and Applied Computer Science, al. A. Mickiewicza 30, 30-059 Krakow, Poland
[c] Institute of Radioisotopes & Radiodiagnostic Products, NCSR "Demokritos", End Patriarchou Gregoriou Str., 15310 Aghia Paraskevi, Greece
[d] Institute of Microelectronics, NCSR "Demokritos", End Patriarchou Gregoriou Str., 15310 Aghia Paraskevi, Greece

ARTICLE INFO

Article history:
Received 10 June 2011
Received in revised form
24 September 2011
Accepted 11 October 2011
Available online 18 October 2011

Keywords:
Immunoglobulins
Amino-organosilane films
Specific binding
Angle-resolved X-ray photoelectron spectroscopy
Atomic force microscopy
Near-field scanning optical microscopy

ABSTRACT

Composition and structure of biorecognition protein layers created on silicon substrates modified with amino-organosilanes determine the sensitivity and specificity of silicon based biosensing devices. In the present work, diverse spectroscopic and microscopic methods were applied to characterize model biosensor surfaces, formed on Si_3N_4 or SiO_2 by modification with (3-aminopropyl)triethoxysilane, coating with rabbit gamma-globulins (IgGs) through physical adsorption, blocking with bovine serum albumin (BSA) and specific binding of an anti-rabbit IgG antibody. In addition, silanized substrates with directly adsorbed BSA or anti-rabbit IgG antibody were examined as reference surfaces. The protein/amino-organosilane/silicon structure of all surfaces was confirmed by X-ray photoelectron spectroscopy. Homogeneity of protein coverage was verified with near-field scanning optical microscope, working in reflection and fluorescence mode. Surface coverage with proteins was determined with angle-resolved XPS using a previously established bilayer approach. Inner structure of protein layers was examined with atomic force microscopy. Vertical arrangement of carbon functional groups was revealed by high resolution ARXPS. Combined spectroscopic and microscopic data reveal the complex character of interactions with the immobilized IgG molecules during blocking with BSA and immunoreaction with anti-IgG antibody. Within experimental error, neither surface coverage nor lateral structural scales of protein layer (provided by Fourier and auto-correlation analysis of topographic and phase images) increase during blocking procedure. On the other hand, coverage and all structural measures rise considerably after immunoreaction. In addition, it was found that polar functional groups orient towards substrate for all protein layers, independently of coverage, prior to and after both blocking and specific binding.

1. Introduction

In recent years, silicon-based micro- and nano-fabrication technology has been successfully combined with biochemistry, enabling fabrication of novel biosensing devices with high sensitivity and selectivity. Different sensing principles have resulted in sensors based on different silicon surface geometries, e.g. nanowires [1], nanoparticles [2], ring cavities [3], cantilevers [4], waveguides [5] and porous films [6]. Such surfaces are usually modified with organosilanes carrying chemically active groups [1–6], such as (3-aminopropyl)triethoxysilane (APTES), to provide a suitable interface between silicon-based transducer and immobilized biomolecules. For sensors where the biorecognition molecule is a protein, silicon surfaces with amino-organosilane films should accommodate these molecules in such a way that their functionality is essentially retained since the sensitivity and specificity of biosensor surfaces depends mainly on that. The immobilization of proteins onto these surfaces can be performed either direct by physical adsorption or after some additional functionalization step via covalent bonding. The first approach remains one of the most popular and efficient ways to immobilize proteins onto solid surfaces despite the increasing number of available covalent bonding methods. Therefore the characterization of silicon surfaces modified with organosilanes prior to and after immobilization of proteins, blocking of free surface sites with a non-functional protein and specific antibody binding is of considerable interest.

The advent and extensions of microscopic and spectroscopic techniques have enabled precise but so far *rather selective*

* Corresponding author. Tel.: +48 12 66 35 550; fax: +48 12 63 37 086.
E-mail address: ufbudkow@cyf-kr.edu.pl (A. Budkowski).
[1] Present address: The Henryk Niewodniczanski Institute of Nuclear Physics, Polish Academy of Sciences, Radzikowskiego 152, 31-342 Kraków, Poland.

0927-7765/$ – see front matter © 2011 Elsevier B.V. All rights reserved.
doi:10.1016/j.colsurfb.2011.10.017

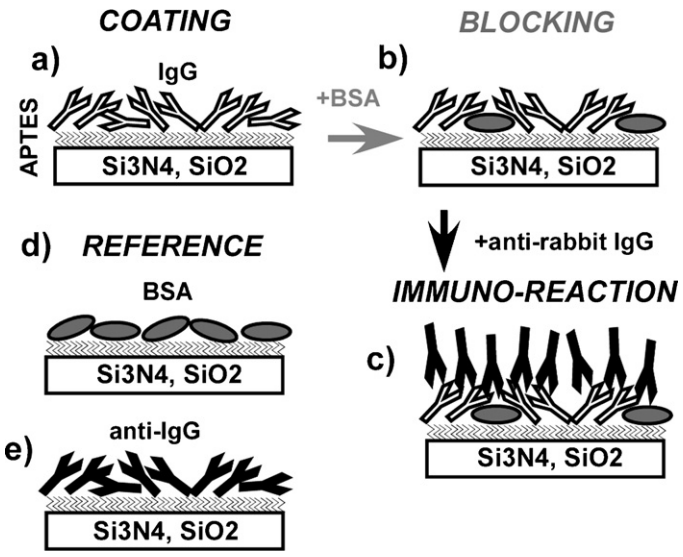

Fig. 1. Schematic representation of model immunosensor Si_3N_4 or SiO_2 surfaces modified with 3-aminopropyltriethoxysilane (APTES) and additional protein layer films formed by successive steps of coating with rabbit IgG (a), blocking with BSA (b) and specific binding of anti-rabbit IgG antibody (c). Silanized substrates coated with BSA (d) and anti-rabbit IgG antibody (e) are used as reference.

characterization of protein nanolayers, such as commonly studied immunoglobulins (IgGs), positioned on amino-organosilane films [7–9,11–13]. Atomic force microscopy (AFM) has revealed with molecular resolution, that lateral IgG nanostructures are changing due to specific antigen–antibody binding [7]. Several AFM studies have shown that such immunoreaction increases also the vertical extent of the protein/organosilane/silicon structure [8,9] but the IgG thickness has not been determined since the tip-scratch method could not be applied to soft substrates [10]. In a previous report, we employed angle-resolved X-ray photoelectron spectroscopy (ARXPS) to determine the amount and thereof the thickness of IgG proteins adsorbed on APTES modified silicon oxide surfaces [12]. As other spectroscopic techniques, ARXPS requires a pre-specified lateral uniformity. The homogeneity of IgG on amino-organosilane spots could be examined with near-field scanning optical microscopy (NSOM) [13], through recording with mesoscopic resolution pairs of topographic and optical (e.g. fluorescence) images at every single surface area. In addition, high resolution ARXPS spectra can reveal preferential orientation of functional groups existing to adsorbed protein molecules towards the substrate [12].

In this work, we present a *complete* characterization of model immunobiosensor surfaces with protein/amino-organosilane/silicon structure by implementing several spectroscopic and microscopic techniques. More specifically, the surfaces are characterized with spectroscopic (XPS, ARXPS) and microscopic (NSOM, AFM) techniques to determine mesoscopic homogeneity, total protein coverage (thickness), lateral nanostructures, and vertical arrangement of functional groups. In addition, lateral structural scales are determined with autocorrelation and Fourier analysis from AFM data independently from topographic and phase images. All these different features were determined for two types of silicon substrates (SiO_2, Si_3N_4) modified with APTES, prior to and after the successive steps of immobilization of rabbit gamma globulins (IgGs), blocking and reaction with an anti-species specific antibody (Fig. 1), in order to mimic the creation of protein layers on a silicon transducer surface during immunoreaction. The impact of blocking and specific antibody binding on the molecular arrangement and makeup of adsorbed protein layers is explicitly discussed.

2. Materials and methods

2.1. Preparation of biosensor surfaces

The substrates used are silicon wafers purchased from Montco Silicon Technologies, Inc. (Spring City, PA, USA). Silicon oxide surfaces were obtained by low pressure chemical vapor deposition of a 1000 nm thermally grown silicon dioxide layer, whereas through an additional deposition of a 150 nm thick silicon nitride layer the Si_3N_4 surfaces were obtained. The amino-organosilane and proteins used to modify both silicon oxide and silicon nitride surfaces were purchased from Sigma Chemical Co., St. Louis, MO, USA. Cleaning and hydrophilization of the substrates were performed with oxygen plasma (using a reactive ion etcher) applied for 30 s under pressure of 10 mTorr and power of 400 W. The hydrophilized surfaces were then immersed in an 0.5% (v/v) 3-aminopropyl(triethoxysilane) (APTES) solution in distilled water for a 2 min, gently washed with distilled water and cured at 120 °C for 20 min.

Model immunosensor surfaces were prepared in successive steps as follows: (a) coating with IgG through incubation with a 0.66 μM rabbit gamma-globulins solution in 0.05 M phosphate buffer, pH 7.4, for 1 h at room temperature (RT), followed by washing with 0.05 M phosphate buffer, pH 7.4, and distilled water, and drying under nitrogen stream; (b) blocking of free-protein binding sites of the surface via immersion in a 10 mg/ml bovine serum albumin (BSA) solution in 0.05 M phosphate buffer, pH 7.4 (blocking solution), for 1 h at RT, followed by washing and drying as described above; (c) immunoreaction through incubation for 1 h with a 0.33 μM solution of anti-rabbit IgG antibody in 0.05 M phosphate buffer, pH 7.4, containing 10 mg/ml BSA, followed by washing with 0.05 M phosphate buffer, pH 7.4, containing 0.05% (v/v) Tween 20, distilled water and drying under nitrogen stream. In addition, reference immunosensor surfaces were obtained by incubating the silanized with APTES substrates with the blocking or anti-rabbit IgG antibody solution following the procedures and conditions described above.

2.2. Microscopic surface characterization

The optical properties of the model immunosensor surfaces at mesoscopic scale were analyzed in air at room temperature using a MultiView 1000 (Nanonics Imaging Ltd., Jerusalem, Israel) microscope with a reflection NSOM set up. The surfaces were illuminated with a laser light (473 nm) using a commercial (Nanonics) metal-coated fiber probe (nominal apical aperture of 100 nm) attached to a quartz tuning fork, which controlled the probe–surface distance. NSOM topographic images were recorded simultaneously with the maps of optical signal. Reflected light was collected by standard objective lens (in far-field region) and then was driven to a photodetector. In addition, when the anti-rabbit IgG antibody used to detect the adsorbed IgGs was labeled with the fluorescent dye AlexaFluor488, the light collected was filtered with the Olympus barrier filter BA515 placed in front to the photodetector. The maps of optical signal were considered meaningful only when the average intensities were higher than 100 Hz (counts per second).

AFM imaging of the model immunosensor surfaces was performed at ambient conditions (air, room temperature) with MultiView 1000 (Nanonics) and Agilent 5500 microscopes working in non-contact mode. The set point and gains were adjusted to obtain minimal noise and clear image of the analyzed surface. For each sample, topography and phase images were acquired simultaneously at several different randomly chosen locations.

Root-mean-square (*RMS*) roughness was determined from AFM images using the software provided along with the AFM instruments, but also using the WSxM free software [14] (downloadable

at http://www.nanotec.es). For each sample its deviations from flat surface were characterized by the mean *RMS* value, averaged from 4 to 7 topographic micrographs. When the average *RMS* roughness was larger than 0.4 nm, then meaningful radially averaged autocorrelation function could be computed for the analyzed surface. This function was expressed by the double value of its width-at-half-maximum (2*WHM*), which can be considered as a measure for the lateral extent of surface features. In addition, their 2-dimensional fast Fourier transforms (FFTs) were calculated from both topographic and phase images. The reversal of wave vector at the maximum of radially averaged FFT spectra ($1/k$) was taken as a characteristic lateral scale of surface structures visible in topographic or phase images.

2.3. Spectroscopic surface characterization

XPS measurements were performed using a VSW Manchester spectrometer with Al Kα radiation (1486.6 eV, 200 W). Angle-resolved XPS spectra were collected for three values of photoelectron take-off angle Θ equal to 0°, 60° and 70°. The operating pressure in the analytical chamber was less than 5×10^{-8} mbar. All XPS peaks were charge referenced to the neutral (C–C) carbon C 1s peak at 284.6 eV. Spectrum backgrounds were subtracted using the Shirley method.

The bilayer model used to determine the thickness of APTES film and the amount (thickness) of immobilized proteins has been described in details in a previous publication [12].

3. Results and discussion

Spectroscopic and microscopic characterization of model immunosensor surfaces (Fig. 1) is performed from different viewpoints. First, the protein/amino-organosilane/silicon structure is verified with XPS (Section 3.1). Second, the uniformity of immobilized protein overlayers is examined with NSOM (Section 3.2). Third, a multilayer extension of ARXPS data analysis is applied to quantify the amount of proteins immobilized after the different steps providing insight about the surface coverage in Section 3.3. Forth, lateral nanostructures in protein overlayers are examined with AFM (Section 3.4). And finally, vertical arrangement of functional carbon groups is determined for all protein layers through analysis with high resolution ARXPS in Section 3.5.

3.1. Protein/amino-organosilane/silicon structure confirmed by XPS

General analysis of photoelectron spectra is a preliminary step to characterize the model immunosensor surfaces after the successive steps, i.e., modification with APTES, coating with rabbit IgG, blocking with BSA and immunoreaction with anti-rabbit IgG antibody. A particularly distinct analysis of these model surfaces is provided by high resolution XPS for the silicon nitride substrates in Fig. 2. In this case, the high resolution XPS spectra of N 1s core-level consist of the signals characteristic for the Si_3N_4 substrate (binding energy of 397.5 eV) but also for amine (NH_2, 399.8 eV) and protonated amino groups (NH_3^+, 401.4 eV).

Silicon surface modification with APTES is performed mainly via APTES hydrolysis followed by surface condensation reaction with the hydroxyl groups of the hydrophilized silicon surfaces, resulting in a film with short APTES hydrocarbon chains terminated with NH_2 groups which point away from the surface siloxane network [17,18]. Attached APTES brushes with such an orientation are characterized by the NH_2 signal in XPS spectra [19,20]. An alternative although less effective coupling mechanism is driven by protonated amino groups pointing towards (charged) silicon [17]. This leads to APTES attachment with reversed orientation (amino groups directed to the surface), manifested in XPS spectra as NH_3^+ signal [19,20]. The contributions from NH_2 and NH_3^+, although less pronounced, are visible in the XPS spectrum in addition to the dominant Si_3N_4 line taken for photoelectron take-off angle $\Theta = 0°$ (upper envelope in Fig. 2a). However, for $\Theta = 70°$ the sampling vertical depth $3\lambda \cos\Theta$ of N 1s photoelectrons is reduced from 8 to 2.7 nm. In this case, the resulting spectrum (lower envelope in Fig. 2a) shows dominant APTES line with amine groups oriented away from the substrate, and negligible contributions from both the silicon nitride substrate and APTES from reversed orientation (NH_3^+).

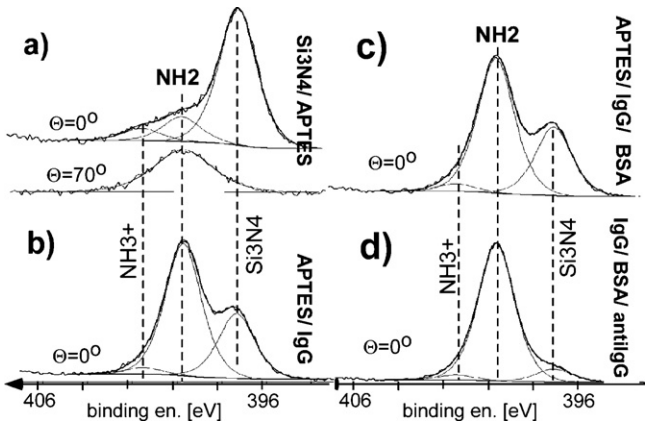

Fig. 2. Vertical composition of model immunosensor Si_3N_4 surfaces analyzed with X-ray photoelectron spectroscopy. N 1s core-level XPS spectra recorded with photoelectrons sampling 8 nm thick regions of analyzed surfaces (sampling vertical depth is reduced to 2.7 nm for take-off angle $\Theta = 70°$ rather than 0°). Distinct contributions from Si_3N_4 substrates and from amine (NH_2 and protonated NH_3^+) groups are visible, characteristic for APTES films (a) and for protein overlayers formed due to successive steps of coating with rabbit IgG (b), blocking with BSA (c), and specific binding of anti-rabbit IgG antibody (d).

The subsequent protein adsorption and detection steps applied to silanized substrate which lead to the creation of protein overlayer, are reflected in the increased contribution of amine groups in the N 1s core-level XPS spectra at expense of reduced Si_3N_4 and NH_3^+ lines, corresponding exclusively to the substrate and the APTES film (cf. Fig. 2a and b–d). Therefore, the creation of protein/APTES/silicon structure on the examined silicon surfaces is confirmed.

In addition, the high resolution N 1s core-level XPS spectra allow for a preliminary comparison of the coated surfaces prior to and after blocking and specific antibody binding. The relative contribution of the NH_2 line attributed mainly to protein attachment to the surface is slightly reduced due to blocking with BSA, whereas the Si_3N_4 signal is somewhat more pronounced in Fig. 2c than in 2b. This suggests the blocking procedure can have a more complex effect on the surface and the already immobilized proteins than the anticipated coverage of the free binding sites of the surface. In contrast, the line from amine groups is considerably increased and the nitride substrate signal diminished in Fig. 2d as compared to Fig. 2c, indicating that the immunoreaction had a great impact onto the surface composition as it was expected from the fact that it leads to the creation of a second protein layer.

3.2. Uniformity of protein overlayers examined with NSOM

Simultaneous collection of topography and optical signal maps, both with high spatial resolution, is the main advantage of surface analysis by NSOM providing a new insight into local arrangement of biomolecules on soft organic substrates [13,15,16]. In the used NSOM set up (Fig. 3), the intensity of light reflected from the analyzed surface was recorded along with topography as a function of

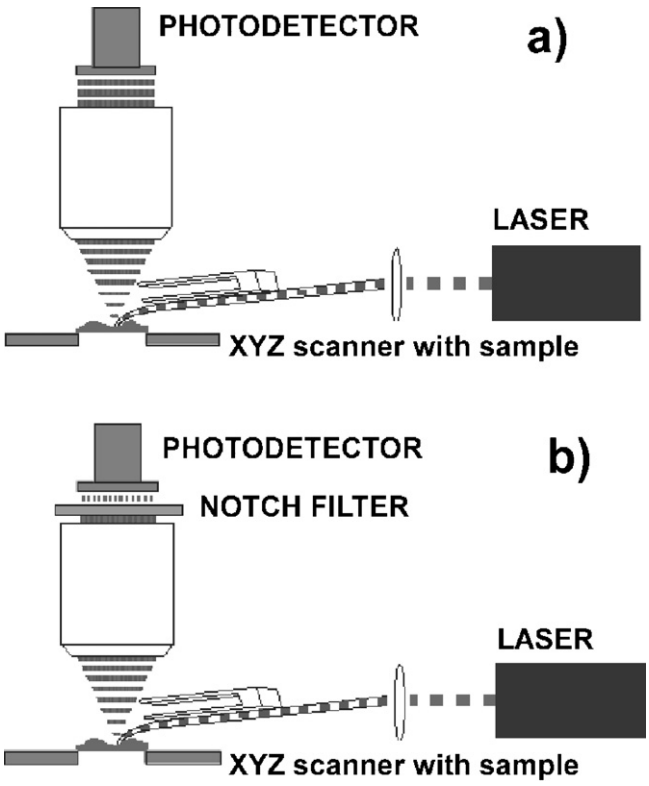

Fig. 3. NSOM (reflection mode) microscopy set up. The optical fiber tip scans across the sample surface at constant nanometer tip-surface distance (controlled by tuning fork), while the surface is illuminated by a sub-wavelength aperture. The light intensity of the whole reflection spectrum (a) or the filtered fluorescence spectrum (b) is recorded as a function of tip position simultaneously with topographic data.

tip position. The surface was 'illuminated' locally with laser light through the scanning NSOM probe with 100 nm aperture, which was kept within a small, sub-wavelength distance from the sample (near field zone), with the distance controlled by a tuning fork. The scanned intensity of light corresponds to the complete spectrum emitted from the analyzed surface ('reflection' mode, Fig. 3a) or to the fluorescence signal of AlexaFluor488 labels attached onto the immobilized anti-rabbit IgG antibody ('fluorescence' mode, Fig. 3b).

Two representative pairs of topography micrographs and scanned intensity maps of 'reflection' spectrum are shown in Fig. 4 for the silicon nitride surfaces after coating with IgG (Fig. 4a and b) and blocking and specific antibody binding (Fig. 4c and d). A uniform spatial distributions of light intensity recorded with mesoscopic NSOM resolution, with image-averaged values (and standard deviations) of 172 ± 81 kHz (Fig. 4b) and 228 ± 50 kHz (Fig. 4d) were determined, which corresponds to relatively small surface height fluctuations with *RMS* roughness of 0.3 nm (Fig. 4a) and 0.7 nm (Fig. 4c), respectively. Since APTES layers on silicon surfaces are homogeneous and their surfaces are featureless [9,12], the results of Fig. 4a–d indicate the uniformity of protein overlayers. Such conclusion is confirmed also by the NSOM results obtained in the 'fluorescence' mode. A pair of topography and scanned intensity map of 'fluorescence' spectrum is presented in Fig. 4e–f for the silanized silicon surface after subsequent exposure to the solutions of rabbit IgG, BSA and anti-rabbit IgG antibody, the later labeled with the fluorescent dye AlexaFluor488. The pair of images shows a uniform film with a singular protein cluster [12] (the left-lower corner in Fig. 4e–f), used as a focal point. Except for this region, the fluorescent light intensity is homogeneous with an image-averaged value equal to 612 ± 178 Hz. This verifies uniformity of (fluorescently labeled) anti-IgG molecules after immunoreaction.

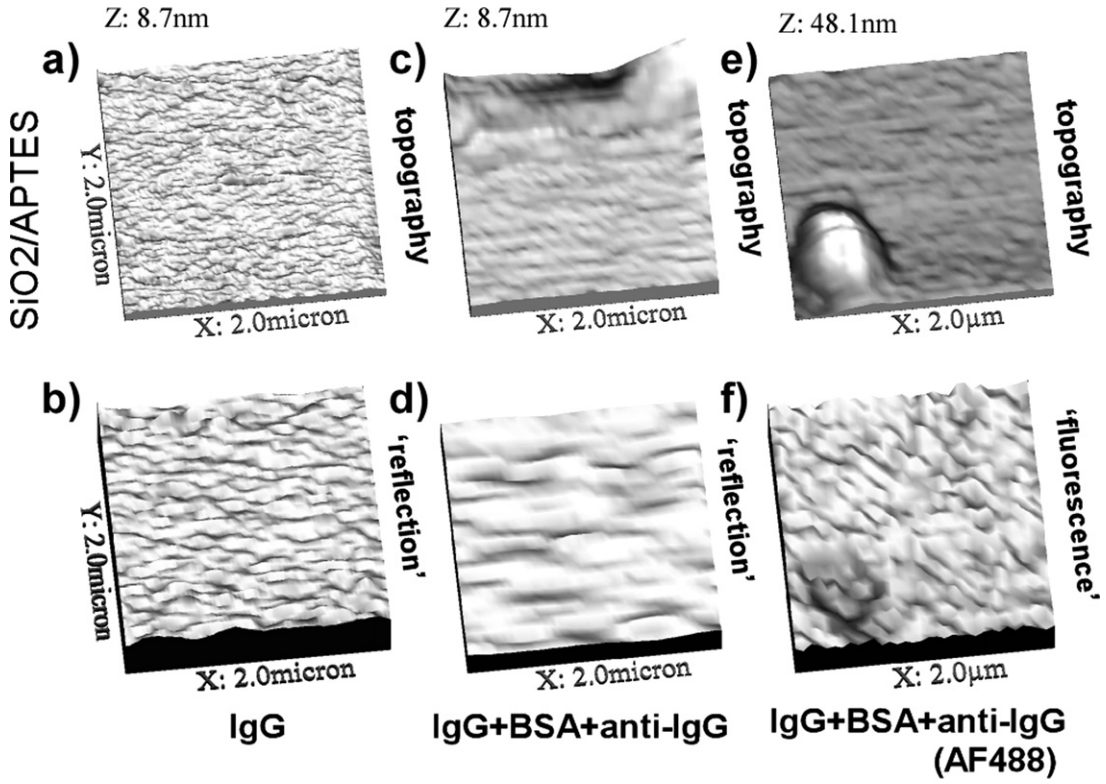

Fig. 4. Uniformity of surface coverage with proteins determined by NSOM. Pairs of topography and light intensity maps (the latter corresponding to reflection or fluorescence spectrum) acquired for SiO_2 substrates modified with APTES and coated with rabbit IgG prior to (a and b) and after blocking and specific binding of anti-rabbit IgG antibody unlabeled (c and d) or labeled with AlexaFluor488 (e and f).

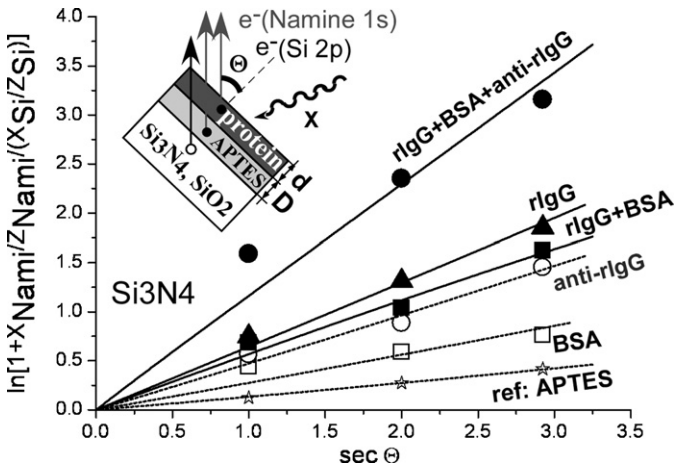

Fig. 5. Multilayer structure (see inset) of model immunosensor surfaces characterized with angle-resolved XPS. The ratio of normalized intensities of the photoelectrons characteristic for APTES film with protein overlayer (N 1s from NH_2 and NH_3^+, see Fig. 2) created on a Si_3N_4 substrate (Si 2p) is plotted versus the take-off angle function sec Θ. The slopes of lines result from regression fitting of individual points and provide the XPS thickness of APTES film and protein overlayer (D and d, respectively, marked in the inset). The inset presents the model used to evaluate the ARXPS data for both Si_3N_4 and SiO_2.

To conclude, NSOM data confirm the uniformity of protein layers, a prerequisite in order to apply the bilayer extension of ARXPS data analysis to determine the surface coverage with proteins.

3.3. Surface coverage with proteins determined with ARXPS

Protein coverage of silicon surfaces modified with APTES can be determined by analysis of ARXPS data using the aminosilane-organic bilayer model, introduced and described in details in our previous publication [12]. Protein coverage or protein surface density can be expressed, after being multiplied by the protein partial specific volume (0.73 cm^3/g), by the thickness d of equivalent protein layer, assuming that the protein is uniformly distributed rather than localized in close packed molecular spheres or ellipsoids [21]. It is this equivalent protein layer that justifies effective attenuation of photoelectrons, and therefore d can be considered as XPS thickness of protein layer.

3.3.1. ARXPS data analysis with bilayer model

The protein/APTES/silicon structure is described by the aminosilane-organic bilayer model, depicted in the inset to Fig. 5. The photoelectrons from amine (NH_2, 399.8 eV) and protonated amino groups (NH_3^+, 401.4 eV) of the N 1s core-level are taken as characteristic for both the APTES film and protein layer, with thickness D and d, respectively, and stoichiometric molar fraction of the atoms emitting characteristic XPS lines Z_{APTES} and Z_{Nami}, respectively. In turn, the photoelectrons from the Si 2p core-level (101.3–102.7 eV) characterize the silicon substrate with stoichiometric Si molar fraction Z_{Si}.

As value for the molar fraction Z_{Nami} for all proteins, we take the atomic concentration (11.0%) determined from XPS analysis of the bulk rabbit IgG material [12]. This assumption seems reasonable for several reasons. First, the anti-rabbit IgG antibody should have similar composition as IgG. Second, the rabbit IgG (and anti-rabbit IgG antibody) molecules constitute the main component of analyzed protein layers. Third, the thickness of directly adsorbed BSA layer (reference) is statistically the same, when the bulk atomic concentration of BSA rather than of IgG is taken for the calculation of Z_{Nami} stoichiometry. The respective molar fractions for APTES and silicon substrate were determined from concentrations of constituent atoms using ARXPS data for the silanized substrates with no protein overlayers, averaged for Θ angles between 0° and 70° [12]. This approach yields values of $Z_{APTES} = 5.4 \pm 1.2\%$ and $Z_{Si} = 31.2 \pm 0.6\%$ for silanized Si_3N_4, and of $Z_{APTES} = 2.6 \pm 0.4\%$ and $Z_{Si} = 32.5 \pm 1.4\%$ for silanized SiO_2. These estimations are reasonable since the Z_{Si} values accord with, for the SiO_2 substrate, or are close to, for the Si_3N_4 substrate, the nominal stoichiometry of SiO_2 surface (33.3%). Low Z_{APTES} values, different for the silicon substrate surfaces, are ascribed to the presence at various amounts of adventitious carbon incorporated in the APTES films [18,22]. The Z_{Si} estimations are reasonable since the values accord with, for the SiO_2 substrate, or are close to, for the Si_3N_4 substrate, the nominal stoichiometry of SiO_2 surface (33.3%). In the case of Si_3N_4 it is expected that oxygen plasma treatment [23] and subsequent silanization in aqueous solution [24] result in simultaneous disappearance of Si–N and increase of Si–O functionality in a nanolayer adjacent to the surface. Formation of such a layer is confirmed by vanishing contribution of Si_3N_4 to the N 1s core-level spectrum for photoelectron sampling depth reduced below 4 nm (i.e., for take-off angle $\Theta \geq 60°$, see Fig. 2a). This is why the stoichiometry of the Si_3N_4 substrate determined with ARXPS resembles that of SiO_2 surface.

Important role in XPS spectroscopy play the normalized photoelectron intensities $X_i = I_i/S_i$, calculated using the sensitivity factors $S_i = \sigma_i \lambda_i$ specified by photoionization cross-sections σ_i [25] and attenuation lengths λ_i [26]. The structural features of the protein/APTES/silicon multialyers are revealed by the ratio of normalized intensities X_i of the photoelectrons (see inset to Fig. 5) characteristic for APTES film with protein overlayer (N 1s from

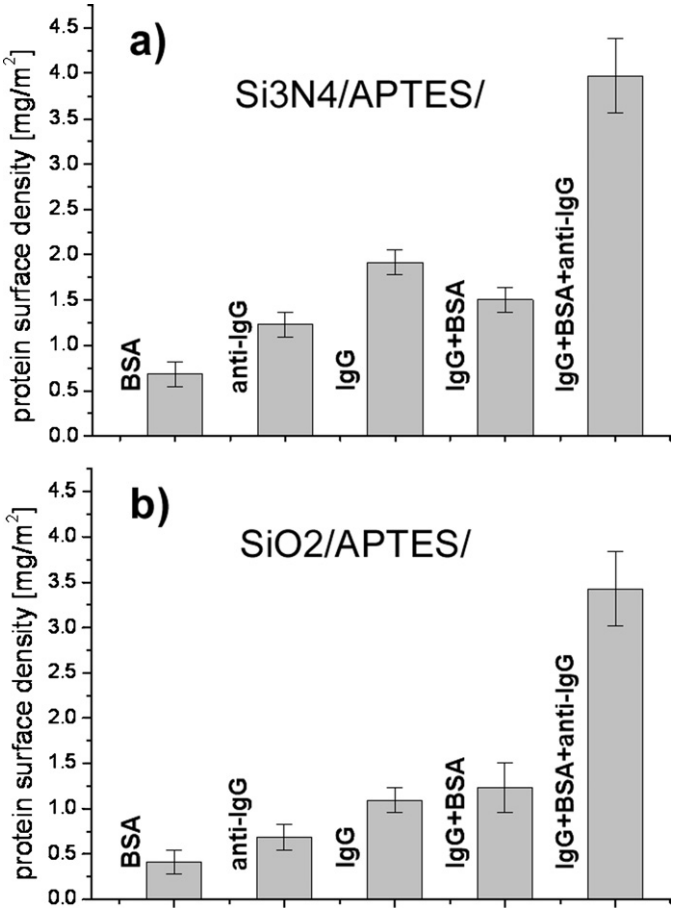

Fig. 6. Protein surface coverage determined from ARXPS data, obtained from silanized Si_3N_4 (a) and SiO_2 (b) substrates coated with BSA or anti-rabbit IgG antibody (reference surfaces) or rabbit IgG. The latter surfaces were blocked with BSA, and reacted with anti-rabbit IgG antibody (model immunosensor surfaces). Error bars are given by the fitting procedure described in Fig. 5.

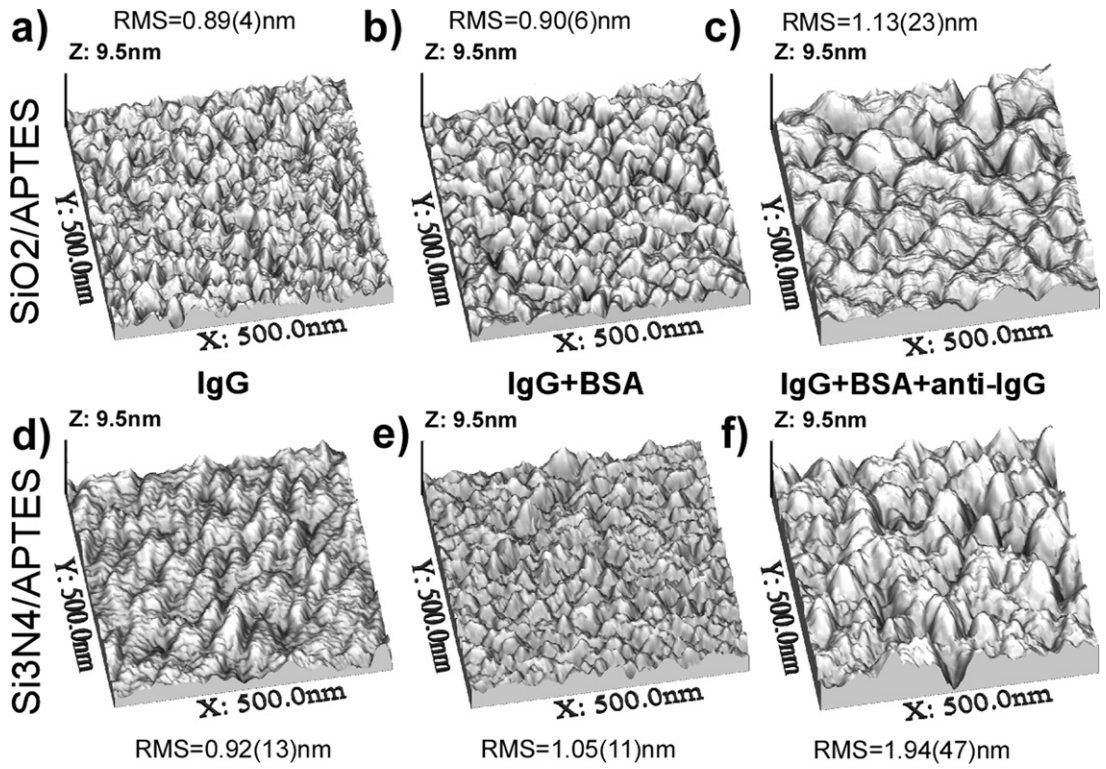

Fig. 7. Lateral topographic structure of protein layers determined with AFM for silanized SiO_2 (a–c) and Si_3N_4 (d–f) substrates after coating with rabbit IgG (a and d), blocking with BSA (b and e), and specific binding of anti-rabbit IgG antibody (c and f). RMS error limits are standard deviations, each determined from 5 images of the same surface.

NH_2 and NH_3^+) and for silicon substrate (Si 2p), calculated by the formula:

$$\frac{X_{Nami}(\Theta)/Z_{Nami}}{X_{Si}(\Theta)/Z_{Si}} = \frac{[1-\exp(-(d\ \sec\ \Theta/\lambda_{Nami}))] + Z_{APTES}/Z_{Nami}[1-\exp(-(D\ \sec\ \Theta/\lambda_{Nami}))]\exp(-(d\ \sec\ \Theta/\lambda_{Nami}))}{\exp(-(D\ \sec\ \Theta/\lambda_{Si}))\exp(-(d\ \sec\ \Theta/\lambda_{Si}))} \quad (1)$$

The ratio of photoelectron intensities is usually plotted in a rearranged logarithmic form versus the take-off angle function sec Θ, as it is shown in Fig. 5. There are two reasons for this. First, the slope of the rearranged formula depends on the total bilayer thickness (D with d). Second, the theoretical (nearly linear) regression fitting of the data in such plots must always start at the origin of coordinate axes, therefore limiting the number of independent data point required. The thickness D of the APTES film was determined in separate ARXPS measurements performed for the two types of silanized silicon surfaces, for SiO_2 was $D = 0.8$ nm and for Si_3N_4 $D = 0.7$ nm. These D values are typical for monomolecular APTES film [17]. With the D values known, the XPS thickness d of protein overlayer remains the only structural fitting parameter of Eq. (1).

3.3.2. Determination of protein coverage

The ARXPS data, shown in Fig. 5 for the Si_3N_4 surfaces, were fitted with Eq. (1) to yield the values of the XPS protein thickness d. The resulting d values are represented as surface coverage of protein layer for silanized Si_3N_4 and SiO_2 in Fig. 6a and b, respectively.

The exposure of the silanized and IgG coated Si_3N_4 surface to the BSA solution results in a slight decrease of protein surface coverage from 1.9 ± 0.1 mg/m^2 to 1.5 ± 0.1 mg/m^2 (Fig. 6a). This suggests not only adsorption of BSA molecules to the surface sites remaining free after IgG adsorption, but also partial exchange of some loosely bound IgG globulins with BSA molecules, which are smaller (with dimensions 14 nm × 4 nm × 4 nm [27] compared with 14.5 nm × 8.5 nm × 4 nm [8] for IgG). Thus after blocking the protein thickness (coverage) of silanized Si_3N_4 surfaces decreases compared to that prior to blocking (see Fig. 6a). Such conclusion is in accord with the results for the SiO_2 series (see Fig. 6b), with surface coverage of 1.1 ± 0.1 mg/m^2 and 1.2 ± 0.3 mg/m^2 prior to and after, respectively, the blocking procedure. In this case, the combined result of covering the free surface sites with BSA and remove of loosely adsorbed IgG molecules leads to statistically indistinguishable protein layer thickness prior to and after blocking.

In contrast to marginal increase or decrease in protein coverage of the IgG coated silicon surfaces, resulting from blocking procedure, their subsequent exposure to the anti-rabbit IgG antibody solution induces a dramatic (~270% in average) increase in protein coverage reaching the value of 4.0 ± 0.4 mg/m^2 for the Si_3N_4 surface (Fig. 6a) and of 3.4 ± 0.4 mg/m^2 for the SiO_2 surface (Fig. 6b). This implies an increase in surface coverage of 2.5 ± 0.5 mg/m^2 and 2.2 ± 0.7 mg/m^2 for the Si_3N_4 and SiO_2 surfaces, respectively, when the anti-rabbit IgG antibodies bind to already adsorbed rabbit IgG. On the other hand, the direct adsorption of the anti-rabbit IgG antibody resulted in an average coverage of 1.2 ± 0.1 mg/m^2 and 0.7 ± 0.1 mg/m^2 for the Si_3N_4 and SiO_2 surfaces, respectively, that are comparable with the values determined for the adsorbed rabbit IgG. This difference can be ascribed to the fact that the directly adsorbed molecules undergo structural deformation during the adsorption process leading to "flattening" of the molecules as compared to their shape in solution. The anti-rabbit IgG molecules, however, retain their natural size to a greater extent since they do not interact directly with the solid surface.

To evaluate additionally how the blocking procedure modifies the exposure of IgG-covered surfaces to anti-IgG antibody

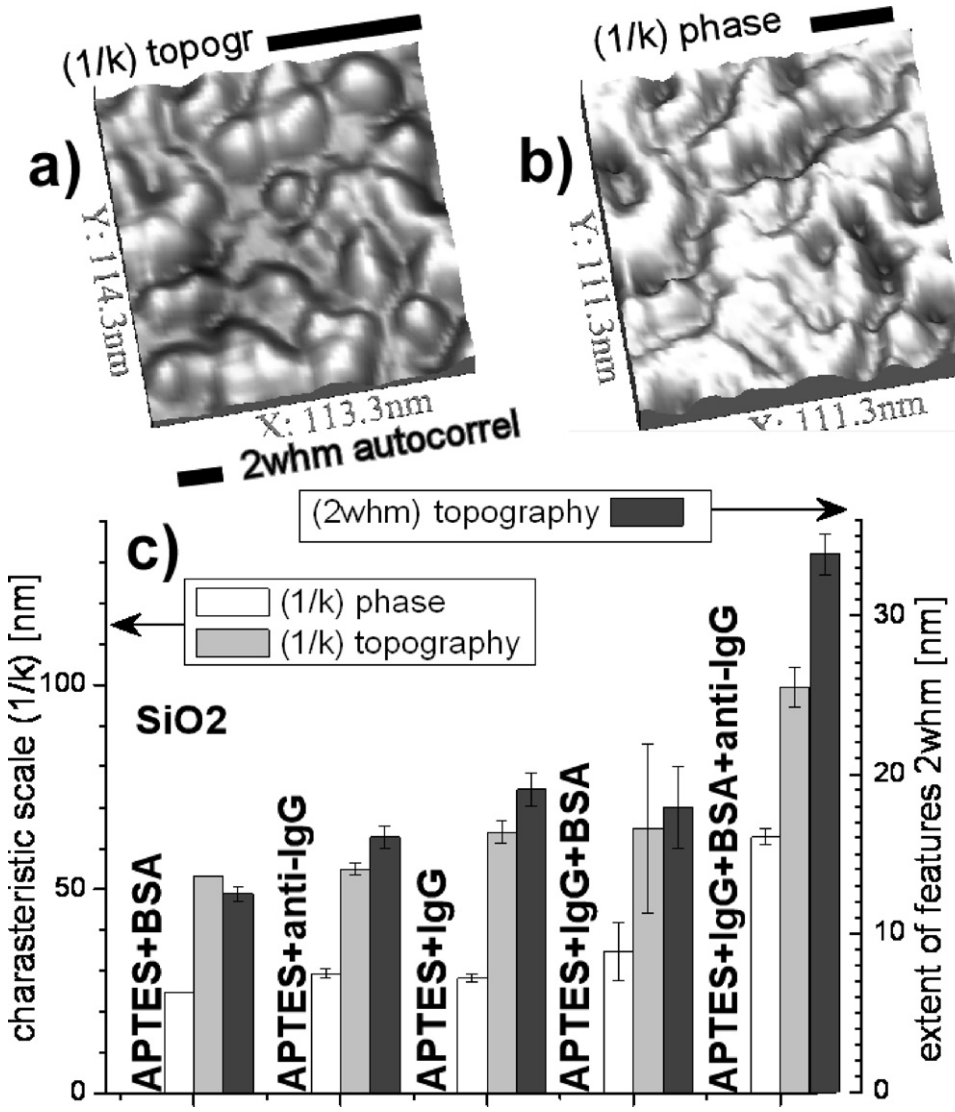

Fig. 8. Topography (a) and phase (b) AFM micrographs of protein overlayers on silanized SiO_2 (illustrated after coating with anti-rabbit IgG antibody) and (c) characteristic scale of surface structures, (1/*k*) (left axis, open and gray columns), determined by Fourier analysis (reversal of wave vector at maximum of radial averaged power spectrum), and spatial extent of topographic surface features, *2whm* (right axis, dark grey columns), calculated by auto-correlation analysis (double-value of width at half-maximum of radial averaged auto-correlation). Error bars are standard deviations, each determined from 5 images.

solution we have performed test experiments for silanized SiO_2 substrates: They showed an increase in protein surface coverage of ~3.4 mg/m^2 for the non-blocked IgG layers exposed to anti-IgG antibody, as compared to the increase of 2.2 mg/m^2 observed for the IgG-covered surface blocked with BSA. This shows that blocking is inevitable to separate immunoreaction from adsorption.

The Si_3N_4 and SiO_2 substrates have similar final surface composition, as revealed by ARXPS (Section 3.3.1). However, their silanization, although performed at identical conditions, resulted in APTES films with different composition. We observe that the protein coverages of the silanized Si_3N_4 surfaces are slightly but systematically larger that those of the silanized SiO_2 substrates (cf. relevant columns in Fig. 6a and b). This is induced by somewhat different composition of APTES film created on these surfaces, as suggested by the higher Z_{APTES} fraction value for the Si_3N_4 surfaces rather than for the SiO_2 ones. The composition impact of APTES film on protein surface density has been confirmed in additional experiments: The silanized Si_3N_4 substrates with reduced Z_{APTES} value (~1.7%) exhibited protein coverage comparable to that observed for SiO_2.

3.4. Lateral structure of protein overlayers examined with AFM

While the overall uniformity of protein layers was indicated by NSOM microscopy (Section 3.1), their inner structure is revealed by AFM. Representative topography micrographs of the model immunosensor surfaces created on silanized SiO_2 and Si_3N_4 substrates after coating with IgG, blocking with BSA and binding of anti-rabbit IgG antibody are presented in Fig. 7. The structure of protein overlayer can be described as a random set of surface features, with specified average feature size and average distance between the features. Apparent IgG molecule radius of 23.5 nm [28] or 18 nm [7] is predicted due to broadening caused by AFM tip (with 20 nm radius) for assumed spherical or half-spherical, respectively, shape of adsorbed IgG globulin with 'real' radius of 7 nm. In turn, intermolecular spacing of about 17 nm or 23 nm is suggested by surface coverage data for the SiO_2 or Si_3N_4 surfaces, respectively, assuming a value of 2.5×10^{-16} mg for the weight of single IgG molecule and an idealized hexagonal molecular arrangement.

The inner structure, visible in AFM images, can be also expressed by the mean value of root-mean-square, *RMS*, roughness of the

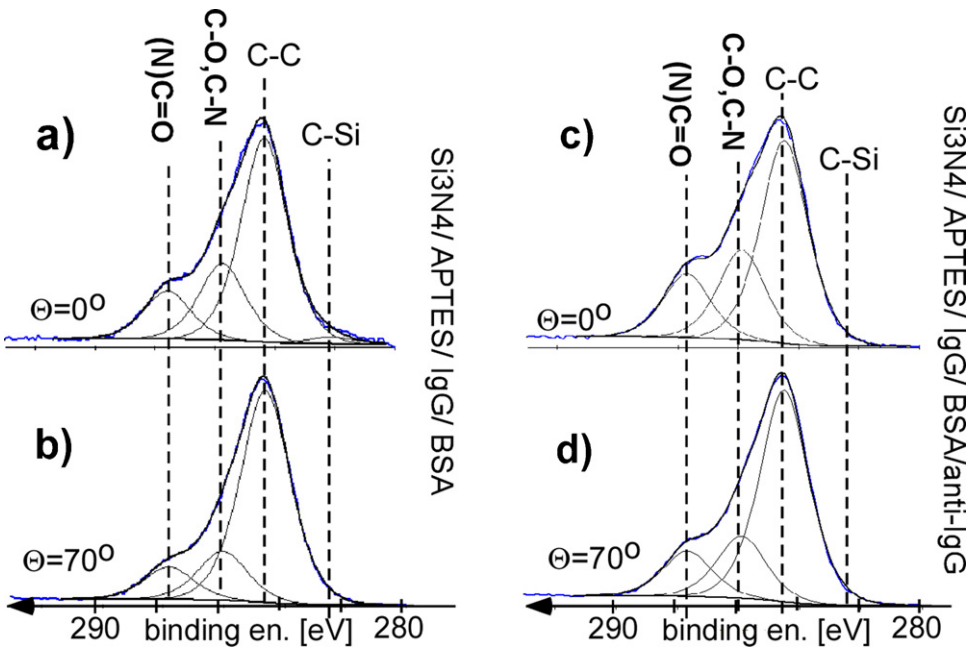

Fig. 9. Vertical arrangement of functional groups analyzed with angle-resolved XPS. C 1s core-level spectra recorded from model immunosensor surfaces with photoelectrons with sampling vertical depths of 8.7 nm and 3.0 nm for take-off angle $\Theta = 0^{\circ}$ and 70°, respectively. Distinct contributions of polar, (N)C=O and C–O or C–N, and non-polar, C–C and C–Si, carbon groups are visible. Representative data (a and b) and (c and d) correspond to situations in Fig. 2c and d, respectively. XPS intensities were rescaled to their maximal values to enable easier comparison between different contributions.

surfaces. Even such a simple measure can reveal interesting features. In particular, for both substrates types, the *RMS* roughness is statistically not affected by blocking procedure but only by immunoreaction as it is shown in Fig. 7. A closer look at Fig. 7a–c and d–f confirms this observation with respect to both the average size of surface feature as well as to the typical distance between the features.

To determine quantitatively the impact of blocking and specific binding on the inner structure of protein overlayer we have applied autocorrelation and Fourier analysis to the AFM data obtained from the SiO_2 surfaces (see Section 2.2 for details). The double-value of the width at half-maximum, *2whm*, of radial averaged autocorrelation provides a measure of the size (extent) of topographic surface feature (Fig. 8a). In turn, reversal of wave vector at maximum, $(1/k)$, of radial averaged power spectrum provides a measure of the distance between the features observed in the topography (Fig. 8a) and phase (Fig. 8b) AFM images. The determined values of lateral scales of protein overlayer inner structure are presented in Fig. 8c. All three structural measures show the same effect of blocking and immunoreaction steps on the inner structure of the adsorbed IgG layer. Within error bars, they are hardly affected by the blocking procedure but are considerably increased by the specific antibody binding.

Let analyze in details the lateral scales presented in Fig. 8. The *2whm* extent of topographic features of immobilized IgG (16–19 nm) accords with apparent radius of IgG molecule (18–23.5 nm). However, the characteristic scales $(1/k)$ of phase (28–25 nm) and topographic (55–65 nm) structures of immobilized IgG are somewhat larger than the spacing (17 nm) suggested by surface coverage data. In addition, the Fourier lengths from topography are twice larger than those from phase micrographs. This suggests that topography AFM images show modulated height of random surface arrangements of immobilized IgG molecules.

Hardly any effect on the three lateral structural scales due to blocking was observed. This can be ascribed to the fact during this step apart from adsorption of BSA molecules to the free surface sites partial exchange of BSA and IgG molecules also occurs (comparable in size except for one dimension [8,27]), as it was concluded in the discussion of surface coverage data (Section 3.3.2). In contrast, the specific binding of anti-rabbit IgG antibodies to the immobilized rabbit IgG molecules induces a dramatic rise in all structural scales: the size, expressed by *2whm*, was increased by ~190% and the distance $(1/k)$ between the surface features by ~165%. These values can be considered along with the even larger increase in surface coverage by proteins by ~280%. A distinct increase upon immunoreaction of the size of the surface features has been reported recently for a human IgG/anti-human IgG antibody interaction [7]. In our case, comparison of the changes in both vertical (surface coverage) and lateral (*2whm*, $1/k$) features magnitude allows an additional insight. The rise in the surface coverage and in the size *2whm* of surface features reflects formation of antigen–antibody complexes, but these complexes are not formed homogeneously across the surface since the distance $(1/k)$ between the surface features also increases. This might be due to the fact that some surface features correspond to BSA rather than IgG molecules. Thus, the anti-rabbit IgG binding to the immobilized IgG molecules occurs in a cluster like way rather than as a homogeneous layer across the surface. This finding is in accordance with the observations of other investigators concerning the creation of "protein islands" during adsorption of IgG molecules onto solid surfaces [29]. In addition, IgG can receive a variety of orientations during their adsorption onto a surface leading to variations in protein layer thickness across the surface [30,31]. Thus, the calculated coverage of SiO_2 (1.1 ± 0.1 mg/m^2) and Si_3N_4 (1.9 ± 0.1 mg/m^2) with immobilized IgG can be compared with the values of 10.1, 5.6 and 2.8 mg/m^2 for the areas covered by singular IgG globulins with head-on, end-on and side-on orientation, respectively. This suggests an immobilized IgG side-on orientation without, however, excluding head-on and end-on orientation at least to some extent.

3.5. Vertical arrangement of polar functional groups revealed by ARXPS

We have previously reported preferential orientation of specific (polar carbon) functional groups towards silicon (SiO_2, Si_3N_4) substrates modified with APTES, observed with XPS and ARXPS for the

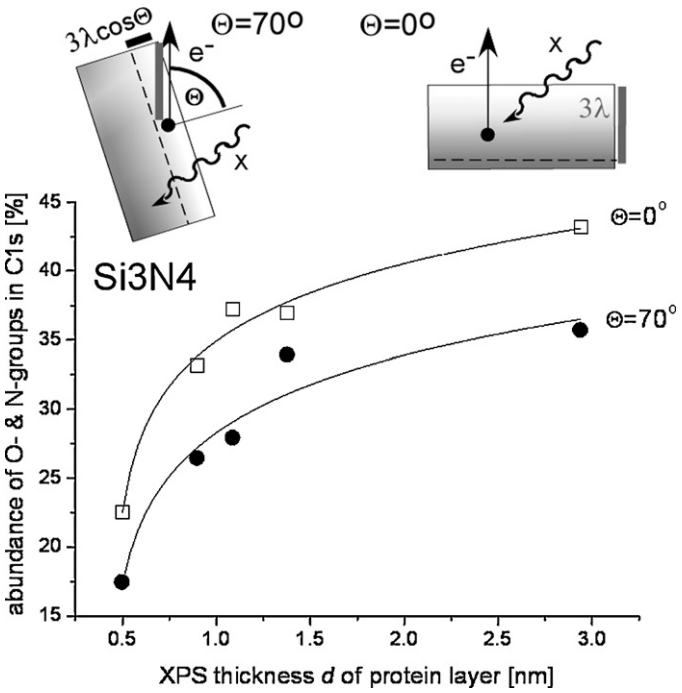

Fig. 10. Fractional contribution of O- and N-containing carbon polar groups to total carbon concentration determined for silanized Si_3N_4 substrate as a function of XPS thickness *d* of protein overlayer. Comparison of the data obtained for photoelectron take-off angle $\Theta = 0^\circ$ (open square, higher sampling depth) and 70° (solid circle) indicates that the polar groups (shaded areas in the inset) are located preferentially closer to the substrate. The solid lines are a guide to eye.

adsorbed layers of rabbit IgG [12]. Here we examine this aspect for all model immunosensor surfaces (Fig. 1). Especially helpful is the analysis of high-resolution ARXPS spectra of the same core-level, where different peaks that correspond to the same element in various functional groups might contribute to a different extent when analyzed as a function of photoelectron take-off angle Θ. Such an analysis is performed for the C 1s core-level spectra, and illustrated in Fig. 9 for the model immunosensor surfaces formed by adsorbing rabbit IgG on silanized Si_3N_4, after blocking with BSA (Fig. 9a and b) and subsequent specific binding of anti-rabbit IgG antibody (Fig. 9c and d). The C 1s envelope can be resolved into four contributions referred to neutral carbon (C–C) at 284.6 eV and three peaks with modified electron environment positioned at 282.1 eV (C–Si), 286.0 eV (C–O, C–N) and 287.9 eV (C=O, NC=O). When the take-off angle Θ is increased from 0° to 70°, then the contribution of polar O- and N-containing carbon groups to the C 1s envelope is visibly reduced in both cases (Fig. 9a, b and c, d).

The effect manifested in Fig. 9 is expressed quantitatively in the form of fractional contribution of polar (O- and N-containing) carbon groups to total carbon concentration determined for two take-off angles $\Theta = 0^\circ$ and 70°, and plotted in Fig. 10 for all model immunosensor Si_3N_4 surfaces as a function of their protein layer XPS thickness *d*. Consistent decrease in the abundance of polar carbon groups, observed for each *d* value when the vertical sampling depth is reduced (higher Θ), indicates that the polar groups are always located preferentially closer to the silanized silicon substrate (see inset to Fig. 10). The solid lines sketched in Fig. 10 are a guide to eye and reflect merely photoelectron attenuation modified by XPS thickness of protein layer.

The results presented in Fig. 10 accord with previous observations of substrate-directed orientation of specific functional groups, which is preserved for the same protein independently of the surface coverage [32,33]. As a completely novel observation, the data in Fig. 10 show that the orientation effect is not only independent of surface coverage, but it is also visible prior to and after both blocking and specific antibody binding. These observations are not unexpected, since the preferential orientation of polar functional groups towards polar substrate is observed for adsorbed rabbit IgG and BSA, then it should be also preserved during adsorption phenomena taking place during blocking of the IgG coated surfaces with BSA [34,35]. Similarly, the preferential orientation, observed for adsorbed rabbit IgG and anti-rabbit IgG antibody, should prevail in the immunocomplexes of rabbit IgG with anti-rabbit IgG antibodies.

4. Conclusions

To conclude, combined spectroscopic (XPS, ARXPS, high-resolution ARXPS) and microscopic (NSOM, AFM) analysis has enabled *complete characterization* of the model immunosensor surfaces (Fig. 1), created by adsorption of a protein/antigen (rabbit IgG) on silicon surfaces (SiO_2, Si_3N_4) previously modified with an amino-organosilane (APTES), prior to and after blocking (with BSA) and immunoreaction (with anti-rabbit IgG antibody). The multilayer protein/amino-organosilane/silicon structure of the surfaces is confirmed with high resolution XPS.

Mesoscopic uniformity is concluded, based on micrograph pairs of topography and light signal provided by NSOM, the latter with image-averaged intensity values larger than 170 kHz, for whole spectrum, or 600 Hz, for fluorescence spectrum of the labeled antibody.

Lateral nanostructures, recorded with AFM are characterized by *RMS* roughness, the size *2whm* of surface features (from autocorrelation) and the distance between them ($1/k$) (from the Fourier analysis) in topography and phase images, independently. It was found that all four measures do not, within experimental error, increase due to blocking procedure but rise considerably after specific antibody binding.

Exactly the same conclusion stems form the analysis of *protein surface coverage* (thickness) data, provided by ARXPS analysis of SiO_2 surfaces. This finding indicates that during the blocking procedure apart from adsorption of BSA molecules to the free surface sites significant role plays the partial exchange of immobilized IgG for smaller BSA molecules. This is further supported by the surface coverage data obtained from the Si_3N_4 substrates.

In turn, the study of immunoreaction effect for the SiO_2 model immunosensor surface, shows rises in the size of surface features *2whm* by ~190% and the distance between them ($1/k$) by ~165%, accompanied by even larger increase in protein surface coverage (~280%). Apparently antigen–antibody complexes are *not* formed at each feature existing in the blocked surface since some of these surface features correspond to BSA rather than IgG molecules.

The surface features visible in topography AFM images reflect modulated height of random surface arrangements of protein molecules. This is suggested by the fact that the Fourier lengths of topography are twice larger than those of phase images. This shows also that phase images obtained in this study are not merely clearer topographical images.

Preferential *vertical arrangement of polar functional groups* towards polar (silanized silicon) substrate is observed with high-resolution ARXPS for all protein nanolayers, independently on surface coverage, prior to and after blocking and specific antibody binding. This orientation effect is preserved not only for nanolayers of different proteins (BSA, IgG, anti-IgG antibody), but also for their mixtures (IgG with BSA) and immunocomplexes (IgG with anti-IgG antibody).

These findings demonstrate the potential of the combined use of different spectroscopic and microscopic methods to throw light on protein layer arrangements on silicon surfaces and thus help to improve the performance of silicon based biosensors.

Acknowledgements

This work was supported by the EU funded project "PYTHIA" (FP7-ICT2-224030). The research was partly carried out with the equipment purchased thanks to the financial support of the European Regional Development Fund in the framework of the Polish Innovation Economy Operational Program (contract No. POIG.02.01.00-12-023/08). One of us (KA) is grateful to financial support (Doctus – Małopolski fundusz stypendialny dla doktorantów) by the European Humans Capital Program.

References

[1] Y. Cui, Q. Wei, H. Park, C.M. Lieber, Science 293 (2001) 1289.
[2] W. Tan, K. Wang, X. He, X.J. Zhao, T. Drake, L. Wang, R.P. Bagwe, Med. Res. Rev. 24 (2004) 621.
[3] K. De Vos, I. Bartolozzi, E. Schacht, P. Bienstman, R. Baets, Opt. Express 15 (2007) 7610.
[4] R. Raiteri, M. Grratarola, H.J. Butt, P. Skladal, Sens. Actuators B 79 (2001) 115.
[5] M. Kitsara, K. Misiakos, I. Raptis, E. Makarona, Opt. Express 18 (2010) 8193.
[6] K.-P.S. Dancil, D.P. Greiner, M.J. Sailor, J. Am. Chem. Soc. 121 (1999) 7925.
[7] Z.J. Lv, J.H. Wang, G.P. Chen, L.H. Deng, Int. J. Biol. Macromol. 47 (2010) 661.
[8] K.-B. Lee, S.-J. Park, C.A. Mirkin, J.C. Smith, M. Mrksich, Science 295 (2002) 1702.
[9] M. Kitsara, P. Petrou, D. Kontziampasis, K. Misiakos, E. Makarona, I. Raptis, K. Beltsios, Microelectron. Eng. 87 (2010) 802.
[10] M. Tencer, R. Charbonneau, N. Lahoud, P. Berini, Appl. Surf. Sci. 253 (2007) 9209.
[11] Y.M. Bae, B.-K. Oh, W. Lee, W.H. Lee, J.-W. Choi, Biosens. Bioelectron. 21 (2005) 103.
[12] K. Awsiuk, A. Bernasik, M. Kitsara, A. Budkowski, J. Rysz, J. Haberko, P. Petrou, K. Beltsios, J. Raczkowska, Colloids Surf. B 80 (2010) 63.
[13] A. Gokarna, Y.H. Kim, Y.-H. Cho, M.S. Lee, I.C. Kang, H.K. Park, M.G. Kim, B.H. Chung, Opt. Rev. 13 (2006) 288.
[14] I. Horcas, R. Fernandez, J.M. Gomez-Rodriguez, J. Colchero, J. Gomez-Herrero, A.M. Baro, Rev. Sci. Instrum. 78 (2007) 013705.
[15] G. Anastasi, G. Cutroneo, A. Pisani, D. Bruschetta, D. Milardi, P. Princi, P.G. Gucciardi, P. Bramanti, L. Soscia, A. Favaloro, J. Microsc. 228 (2007) 322.
[16] N.E. Dickenson, K.P. Armendariz, H.A. Huckabay, P.W. Livanec, R.C. Donn, Anal. Bioanal. Chem. 396 (2010) 31.
[17] J. Kim, P. Seidler, L. Sze Wan, C. Fill, J. Colloid Interf. Sci. 329 (2009) 114.
[18] J.A. Howarter, J.P. Youngblood, Langmuir 22 (2006) 11142.
[19] D. Kowalczyk, S. Slomkowski, M.M. Chehimi, M. Delamar, Int. J. Adhes. Adhes. 16 (1996) 227.
[20] M.R. Horner, F.J. Boerio, H.M. Clearfield, J. Adhes. Sci. Technol. 6 (1992) 1.
[21] E.N. Vasina, E. Paszek, D.V. Nicolau Jr., D.V. Nicolau, Lab Chip 9 (2009) 891.
[22] E. Strein, D. Alfred, Thin Solid Films 517 (2008) 1011.
[23] C. Jiménez, J. Perriére, I. Vickridge, J.P. Enard, J.M. Albella, Surf. Coat. Technol. 45 (1991) 147.
[24] T.J. Senden, C.J. Drummond, Colloid Surface A 94 (1995) 29.
[25] J.H. Scofield, J. Electron. Spectrosc. 8 (1976) 129.
[26] D. Briggs, Surface Analysis of Polymers by XPS and Static SIMS, Cambridge Univ. Press, Cambridge, 1998.
[27] Y.L. Jeyachandran, J.A. Mielczarski, E. Mielczarski, B. Rai, J. Colloid Interface Sci. 341 (2010) 136.
[28] O. Ouerghi, A. Touhami, A. Othmane, H. Ben Ouada, C. Martelet, C. Fretigny, N. Jaffrezic-Renault, Biomol. Eng. 19 (2002) 183.
[29] C. Zhou, J.-M. Friedt, A. Angelova, K.-H. Choi, W. Laureyn, F. Frederix, L.A. Francis, A. Campitelli, Y. Engelborghs, G. Borghs, Langmuir 20 (2004) 5870.
[30] S. Chen, L. Liu, J. Zhou, S. Jiang, Langmuir 19 (2003) 2859.
[31] B. Lu, M.R. Smyth, R. O'Kennedy, Analyst 121 (1996) 29R.
[32] J.A. Mielczarski, J. Dong, E. Mielczarski, J. Phys. Chem. B 112 (2008) 5228.
[33] M.M. Browne, G.V. Lubarsky, M.R. Davidson, R.H. Bradley, Surf. Sci. 553 (2004) 155.
[34] M. Mrksich, G. Whitesides, Annu. Rev. Biophys. Biomol. Struct. 25 (1996) 55.
[35] M. Rabe, D. Verdes, S. Seeger, Adv. Coll. Int. Sci. 162 (2011) 87.